Military Technical College
Kobry El-Kobba
Cairo, Egypt

12-th International Conference
on
Aerospace Sciences &
Aviation Technology

CONTRIBUTION TO THE DEVELOPMENT OF IN718 ALLOY

N. El-Bagoury*, A. Nofal*, K. Yamamoto**, H. Miyahara** and K. Ogi**

I. Nickel base Superalloys and the Aerospace Industries

"Superalloys" is a generic term usually applied to alloys based on group VIII elements (Fe, Ni and Co) developed for high temperature (〉550°C) applications under sever mechanical stressing. These alloys are highly resistant to oxidation, hot corrosion and erosion as well as microstructural degradation. Superalloys are usually used up to a higher proportion of their actual melting point compared to other metallic materials. Aero engines have been over years the prime driving force for the development of superalloys. Other users of superalloys include marine, space vehicles, rocket engines, nuclear reactors, steam power plants and petrochemical equipment.
Over the past four decades, new alloys have been explored to meet specific material property requirements of aeronautical industry:

- High creep and stress rupture strengths at elevated temperatures.
- High tensile and proof strengths at operating temperatures.
- High oxidation and hot corrosion resistance.
- Microstructural stability.
- Resistance to crack propagation and
- Low notch-sensitivity under various loads.

I. 1. Metallurgical Principles of Ni-Superalloys

In addition to solution strengthening imparted by alloying with Cr (up to 30%) and/or molybdenum, precipitation hardening from solubility difference with temperature of two unique intermetallic compounds:

- Gamma prime, γ' {Ni_3(AL, Ti)} and
- Gamma double prime γ'' (Ni_3Nb).

The Ni superalloys contain Al, Ti or Nb mostly in combination to result in the precipitation of γ' or γ'' or $\gamma'+\gamma''$ as the second phase. Solution and precipitation heat treatment induce the uniform precipitation of these intermetallic compounds, which significantly increases the mechanical properties of the alloy over a range of temperatures. The response to

*** CMRDI, Cairo, EGYPT.**
**** Faculty of Engineering, Kyushu University, JAPAN.**

precipitation hardening temperatures may be delayed by the addition of Nb in alloys such as IN718 leading to improved weldability as the heat of welding would not induce hardening at consequent post-weld cracking.
Strength of superalloys is usually enhanced through addition of alloying elements, which may act as:

- Solution strengthening elements such as Cr, W, Mo and Ta.
- Precipitation strengthening as γ' and/or γ'' forming elements such as Ti, Al and Nb.
- Grain boundary strengtheners e.g. C, B, and Zr may be added for elevated temperature properties.

Current Ni Base Superalloys are rather complex and require sophisticated production facilities. Their use extends to the highest temperature of any common alloy systems. Presently, they comprise over 50% of the weight of advanced aircraft engines. The influence of alloying as well as trace elements has been the subject of extensive investigation aiming at controlling these elements through different combinations of melting routes to have optimum properties for highly stressed aeroengine components. Moreover, work on structure-property correlations is of special importance since degradation of structure with time results in determination of properties and this affecting the life of components used at elevated temperatures (650-1100°C).
Table (1) shows the chemical compositions of some of the most widely used heat resistant Ni base casting alloys. [1]

Table (1) chemical compositions of some of heat resistant Ni base casting alloys. [1]

Alloy designation	Nominal composition, %											
	C	Ni	Cr	Co	Mo	Fe	Al	B	Ti	W	Zr	Others
B-1900	0.1	64	8	10	6	...	6	0.015	1	...	0.10	4Ta(a)
CMSX-2 (SC)	<30 ppm	66	8	4.6	0.6	...	5.6	...	1.0	8	...	6.0Ta
CMSX-3 (SC)	<30 ppm	66	8	4.6	0.6	...	5.6	...	1.0	8	...	6.0Ta, 0.10Hf
CM-247-LC (SC)	0.07	62	8.1	9.2	0.5	...	5.6	0.015	0.7	9.5	0.015	3.2Ta
HW(b)	0.55	60	12	...	0.5	23	...	...	...	...	...	2.0Mn, 2.5Si
HX(b)	0.55	66	17	...	0.5	12	...	...	...	...	...	2.0Mn, 2.5Si
Alloy X	0.1	50	21	1	9	18	...	...	...	1	...	...
Alloy 100	0.18	60.5	10	15	3	...	5.5	0.01	5	...	0.06	1V
Alloy 738X	0.17	61.5	16	8.5	1.75	...	3.4	0.01	3.4	2.6	0.1	1.75Ta, 0.9Nb
Alloy 792	0.2	60	13	9	2.0	...	3.2	0.02	4.2	4	0.1	4Ta
Alloy 713C	0.12	74	12.5	...	4.2	...	6	0.012	0.8	...	0.1	2Nb
Alloy 713LC	0.05	75	12	...	4.5	...	6	0.01	0.6	...	0.1	2Nb
Alloy 718	0.04	53	19	...	3	18	0.5	...	0.9	...	...	0.1Cu, 5Nb
Alloy X-750	0.04	73	15	...	...	7	0.7	...	2.5	...	...	0.25Cu, 0.9Nb
M-252	0.15	56	20	10	10	...	1	0.005	2.6	...	...	...
MAR-M 200 (DS)	0.15	59	9	10	...	1	5	0.015	2	12.5	0.05	1Nb(c)
MAR-M 246	0.15	60	9	10	2.5	...	5.5	0.015	1.5	10	0.05	1.5Ta
MAR-M 247 (DS)	0.15	...	9.4	10	0.7	...	5.5	0.015	1	10	0.05	1.5Hf, 3Ta
NX 188 (DS)	0.04	74	...	...	18	...	8	...	...	...	...	...
René 77	0.07	58	15	15	4.2	...	4.3	0.015	3.3	...	0.04	...
René 80	0.17	60	14	9.5	4	...	3	0.015	5	4	0.03	...
René 100	0.18	61	9.5	15	3	...	5.5	0.015	4.2	...	0.06	1V
TRW-NASA VIA	0.13	61	6	7.5	2	...	5.5	0.02	1	6	0.13	0.4Hf, 0.5Nb, 0.5Re, 9Ta
Udimet 500	0.1	53	18	17	4	2	3	...	3	...	...	...
Udimet 700	0.1	53.5	15	18.5	5.25	...	4.25	0.03	3.5	...	...	...
Udimet 710	0.13	55	18	15	3	...	2.5	...	5	1.5	0.08	...
Waspaloy	0.07	57.5	19.5	13.5	4.2	1	1.2	0.005	3	...	0.09	...
WAZ-20 (DS)	0.20	72	...	...	...	...	6.5	...	...	20	1.5	...

(a) B-1900 + Hf also contains 1.5% Hf. (b) AC1 designation. (c) MAR-M 200 + Hf also contains 1.5% Hf.

I. 2. Aerospace Applications of Ni Superalloys

The development stages of Ni superalloys for aerospace applications may be summarized in the following:

- At the beginning, the Ni superalloys evolved as forgeable alloys.

- Higher additions of γ' strengtheners were later added to improve the higher temperature strength.
- Continual increase of these elements and the accompanied higher volume fraction of γ' made the alloys difficult to forge, resulting in evolution of sophisticated casting techniques.
- To increase the performance at still higher temperatures, design modifications were carried out to introduce cooling channels in blades and develop hollow components to facilitate cooling of material by air.
- Elimination of grain boundaries in direction of stresses in directional solidification technology (DS) resulted in further improvement in material capability at higher temperatures.
- Ultimately, the development of mono crystal or single crystal (SC) technology gave little space for further improvement.

Recent research work on refractory metals, intermetallic and ceramic components loss has shown tremendous potential as aerospace materials, but their use can be possible if combinations of properties would satisfactory minimum design requirements. Till then, Ni base superalloys are expected to continue domination even for advanced turbine applications due to:

- Favorable property combination.
- Proven production capabilities.
- Operating capabilities extend up to 90% to 95% of their absolute melting point.
- Rapid development of sophisticated air cooling design extending from polycrystalline to directionally solidified and monocrystal blades to combat higher turbine entry temperatures.
- Effectiveness of thermal barrier coatings to raise insulation benefit by 100-200°C.

I. 3. Inconel 718 Superalloy

The interest in IN718 as aircraft engines material dates back to 1960's, where new jet engines were under development at GE for the Supersonic Transport (SST) and the Air Force's C-SA, the first of the wide –body air planes. [2] Later on, IN718 became the most widely used superalloy for aerospace applications such as the critical rotating parts, airfoils, supporting structures and pressure vessels.

Parallel to the development efforts made by GE:-
The early sixties, Pratt and Whitney (P&W) started to introduce the alloy IN718 as a material for the gas turbine engine, enabling the manufacture of engines with lower cost, lighter weight and simplified construction. The applications and evolution of this unique material was recently traced in the past four decades at P&W along with some of the reasons for its introduction. [3] This report shows that from its initial use in 1963 for the diffuser case of the J 58 engine for the SR-71 Blackbird, the alloy is now the most widely used of all Ni-alloys at P&W. Applications include disks, cases, shafts, blades, stators, seals, supports, tubes and fasteners.

Continued growth of IN718 application base has been fostered by both business as well as technical characteristics:

- Multiple manufacturing processes and product forms have been developed over years due to the relative manufacturing ease.
- Slow precipitation kinetics offers a weldability advantage which is important for reduction in manufacturing losses and field repair.
- A large material supplier and fabricator base has evolved as a result of the free license to manufacture.
- Investment cast IN718 has been extensively utilized in the structural design of aircraft engines to reduce the cost of fabricated components.

Today, the attractive physical metallurgy and the large utilization base of IN 718 make it the logical first choice for the scale- up of new, low cost manufacturing methods. The current applications of the alloy are however limited by the meta-stability of the γ" strengthening system at high temperatures. Engine design engineers are demanding developed versions of IN718 with higher temperature. The second part of this document demonstrates some of the efforts made at CMRDI in this direction. The success of these trials will certainly rely on the well-coordinated efforts with the concerned aerospace industry in the country.

IN718 was first introduced into a production application for parts of the J93 (XB-70 bomber engine) turbine frame that were welded to wrought IN722 rings at GE. The next application led to significant production outlet; the GE1 development core evolved to GE's successful, long running TF39/CF6-6/LM2500 engine family. Selection of 718 forgings for compressor airfoils, critical rotating hardware, and static structures required fast-paced, focused efforts at General Electric Aircraft Engines (GEAE) and its supplier base to ensure success in the TF39 engine program, as well as in the CF6-6 and LM2500 derivatives.

Figure 1 shows that Alloy 718 comprises a striking 34% of finished component weight of a typical CF6 engine. The usage is distributed over forgings and investment castings.

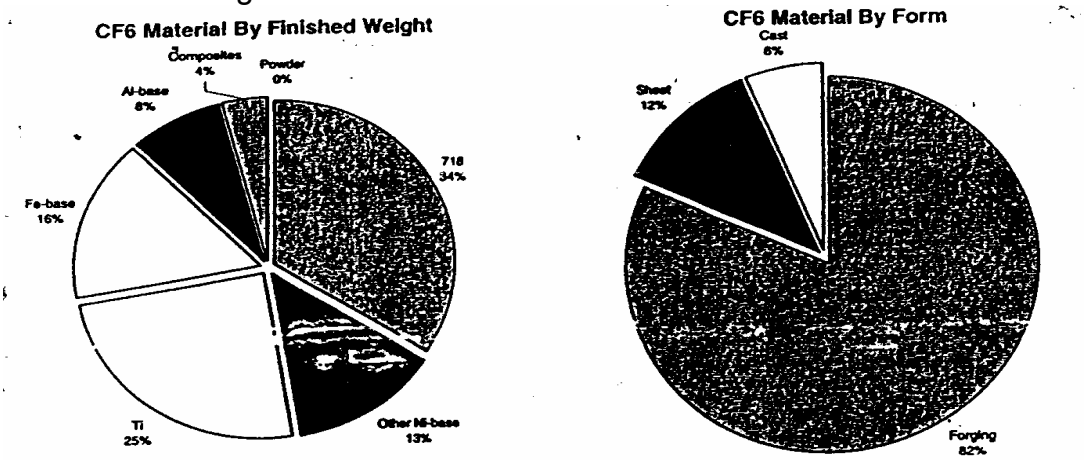

Fig. 1 Alloy 718 relative input weights for a typical CF6 configuration.[3]

Further enhancement of the alloy's property balance and reproducibility was achieved by optimizing the process parameters. Major advances may be related to developments in ingot melting methods that dramatically improved cleanliness, minimized ingot defects such as freckles and reduced segregation, enabling the casting of larger diameter ingots. Still more accelerated rate of application of the alloy into more critical engine components was possible due to improvements in billet conversion and forging methods leading to finer grain products and improved sonic inspectability.

Significant weight benefits could be realized with a higher strength modification of IN718 for large structural casting applications such as diffuser cases. Composition modifications consisted mainly of raising the Ti content to 2% and the Nb content to 6% while lowering the Cr content from 17% to 12% leading to about 25% increase in yield strength and creep- rupture properties approaching those of wrought materials.

The challenge, however, remains to achieve wrought property levels through use of lower cast processes. Some of the major process technologies with real potential foe achieving wrought property levels include powder injection molding (PIM) and vacuum die casting for high volume, relatively small but complex configurations such as compressor airfoils and brackets.

II. Development of IN718 Alloy at CMRDI

II. 1. Introduction

Inconel 718 (IN718) is a nickel-base superalloy widely used in the fabrication of critical pieces for turbine engines, because of its higher yield strength up to 923K, and excellent impact strength and fracture toughness down to 233K, as well as good corrosion resistance.[4] Recently, refractory elements are utilized to increase high temperature strength and creep resistance of Ni base superalloys.[5] Among the refractory elements Re is a particularly effective strengthener, which partitions selectively to the γ phase and acts as a γ' coarsening retarder.[6, 7] However, excessive addition of refractory elements may result in thermosolutal convective instabilities during solidification and might cause defects such as macro-segregation, freckles, laves phase and white spots.[8] While most parts of IN718 are produced at slow cooling rates as precise casting products, some are produced at high cooling rates, and sometimes cast defects are repaired by arc welding.[9] Though the relationship between microstructure and mechanical properties for cast alloy IN718 has been discussed by many investigators, [10, 11, 12] quite few researches are made on the influence of Re and cooling rate on solidification phenomenon. Therefore, the solidification structures and Re distribution were investigated in IN718 containing 2-6% Re cooled at 1- 100 K/min.

II. 2. Effect of Re on Solidification of Standard IN718 Alloy

The solidification of Standard IN718 (St-IN718) proceeds in the order of: primary γ, eutectic(γ+NbC) and (γ+Ni_2Nb). These three stages were found also with Re containing alloys but at different temperatures.

The influence of Re on the liquidus temperature and the other phase transformation temperatures are presented in Fig. 2. As shown in this figure, the liquidus temperature of St-IN718 is 1613K, [11] this temperature elevates gradually to 1638K with the increase in Re to 6 %.
In addition to the liquidus temperature, both the eutectic (γ+NbC) and (γ+Ni_2Nb) transformation start temperatures become higher from 1562K to 1586K and from 1448K to 1478K with the increase in Re content to 6%, respectively.
Fig. 3 shows the solidification microstructure of the Re-containing IN718 cooled at 10 K/min. The microstructure consists of primary γ, eutectic (γ+NbC) and eutectic (γ+Ni_2Nb), just like the case of St-IN718. Both EPMA photographs, BSE and RE images, are used to distinguish NbC from Ni_2Nb phase. Through BSE image, both NbC and Ni_2Nb show a similar bright structure, however in RE image on polished surface, NbC gives more brightness than Ni_2Nb because of higher hardness of NbC. The γ phase was solidified as a primary with dendrite morphology from the liquid during the solidification process. Both of eutectic (γ+NbC) and eutectic (γ+Ni_2Nb) were found to form later in the interdendritic regions, as shown in Fig. 3.

As the comparison of microstructures of St-IN718 and Re containing alloys cooled at 10K/min, indicated that the dendrite arms become larger by the addition of Re content, the secondary dendrite arm spacing (SDAS) was measured on each specimen. As shown in Fig. 4, the SDAS expands with the increase in Re content as represented in the following equation:

SDAS (um) = 3.5 Re% + 60.3 ……. (1)

The volume fractions of primary γ**,** eutectic **(**γ+NbC) and eutectic **(**γ+Ni_2Nb) phases varied depending on Re content. As shown in Fig. 2, volume fraction of primary γ is 0.71 in St-IN718, [12] which increased significantly to 0.83 by the addition of 6% Re. Therefore, the volume fraction of the residual liquid for the further phase transformations decreased, and the eutectic (γ+NbC) and (γ+Ni_2Nb) in St-IN718 were lowered from 0.21 to about 0.13 and from 0.08 to 0.04, respectively.

As for the Ni_2Nb phase, many researchers recently reported that the volume fraction of Ni_2Nb phase would become higher as the Re content increase in Ni base superalloys.[7, 11] However, the Ni_2Nb phase volume fraction in St-IN718 decreased from 2.5% to 2.2 as the Re% increased to 6%, as shown in Fig. 4.

II. 3. Influence of cooling rate on solidification mode and structure

The microstructure of the alloy consists of dendritic primary γ, eutectic (γ+NbC) and eutectic (γ+Ni_2Nb) distributed in the inetrdendritic regions. The experimental alloy crystallizes in the order of primary γ, eutectic (γ+NbC) and eutectic (γ+Ni_2Nb). As shown in Fig. 5, the liquidus temperature of primary γ decreases from 1636K to 1615K by increasing the cooling rate from 1K/min to 100K/min. In addition, the eutectic temperatures of (γ+NbC) and (γ+Ni_2Nb) phases are reduced to 1567K and 1406K from 1587K and 1502K, respectively. The temperatures of nucleation of primary γ and eutectic phases are generally influenced by the cooling rate. Thus these equations are obtained in this experiment conditions.

(a) primary □

$$T_{□} = 0.21 \text{ Log } (V) \quad \text{.... (1)}$$

(b) □ + NbC

$$T_{□ + NbC} = 0.20 \text{ Log } (V) \quad \text{.... (2)}$$

(c) □ + Ni_2Nb

$$T_{□ + Ni2Nb} = 0.42 \text{ Log } (V) \quad \text{.... (3)}$$

Where, V is cooling rate (K/min).
The plotted data of eutectic (□ + Ni_2Nb) has higher slope than other slope lines.

Fig. 6 clarify the influence of cooling rate on microstructure, the secondary dendrite arm spacing of primary γ (SDAS, $_{2}$ [□m]) has been measured using the EPMA photography. The relationship between SDAS and cooling rate (V [K/min]), shown in Fig. 7, is represented by the following equation:

$$\lambda_2 = 145.5\ V^{-0.3} \quad \text{.... (4)}$$

The SDAS decreases from 154.9 to 36.1 μm as the cooling rate increases from 1 K/min to 100 K/min. The cooling rate may also influence the volume fraction of NbC and Ni_2Nb phases. However, it was difficult to distinguish between NbC and Ni_2Nb phases, because NbC and Ni_2Nb look similar on the etched surface in optical microscope and on composition image in EPMA, Fig.3 (a). Therefore, we utilized the hardness difference between NbC and Ni_2Nb Phase. Figure 3 (b) shows the secondary electron micrograph, which indicates roughness of a specimen surface. NbC phase surface rose up because of its high hardness while Ni_2Nb phase flattened on the polishing surface. Depending on the difference between these two kinds of photographs, it was easy to measure the volume fraction (V_f) of both NbC and Ni_2Nb phases. As shown in Fig. 8, the volume fraction (V_f) of NbC and Ni_2Nb are expanded by increasing the cooling rate. The NbC phase was found at all cooling conditions and slightly increased from 1.0% at 1K/min to 1.6% at 100K/min. While the Ni_2Nb phase almost ceased to exist, V_f=0.02%, at the slowest cooling rate of 1K/min and expanded to 3.64% of 100K/min, in 3.5% Re IN718 alloy. The V_f of both NbC and Ni_2Nb phases of standard IN718 are higher than in 3.5% Re IN718 alloy. This could be related to the effect of adding Re. As the 3.5% Re added to the standard IN718 alloy, the Nb concentration in the same alloy is decreased. In addition, the volume fraction of primary γ phase is increased by the additions of 3.5% Re to standard IN718 alloy. [13]

II. 4. Redistribution of elements in primary γ and liquid phase

The redistribution of elements in the primary γ phase was investigated under variant cooling conditions. Figure 9 demonstrates the concentrations profile of Nb and Re in γ phase from the center to edge of γ phase dendrite with different cooling rates. At the center of γ phase dendrite, the Nb concentration is the lowest and Re concentration is the highest. By going away from the dendrite center, the Nb concentration starts to elevate and Re concentration decreases reaching their highest and lowest concentrations at the border of

the γ phase dendrite, respectively. Re selectively segregates to primary γ while Nb prefers to diffuse towards the inetrdendritic regions. As shown in Fig. 10, the concentration of Nb for 1 K/min is obviously differing from the 100 K/min cooling rate at the γ dendrite center. The Nb concentration, related to 1 K/min is higher than 100 K/min at the center of γ dendrite. This concentration is increased away from the center of dendrite gradually in case of 1 K/min while it is increased with higher inclination in case of 100 K/min. But the effect of cooling rate on the diffusion of Re in solid γ is slightly lower than in case of Nb. At the center of the γ dendrite, there is an interaction between the concentration of Re with 1 and 100 K/min. This interaction is lowered by going away from the dendrite center and became clearly differing at the dendrite boundary. The slope of Re concentration is higher for 100 K/min in comparison with 1 K/min, especially in the area adjacent to the dendrite boundary. According to A. D. Patel and Y. V. Murty, [13] and Wanhong Yang et al. [14], at lower cooling rates, there is enough time for back diffusion in the solid (solidification time is greater than diffusion time); hence, a lower fraction of eutectic laves (Ni_2Nb) phase forms. This suggests that in large ingots, the volume fraction of laves phase is the highest at the surface of ingot and decreases towards the central part. This statement agrees with our results for the V_f of Ni_2Nb versus the cooling rate in Fig. 8.

In order to evaluate the back diffusion of solute elements in sloid γ phase, Scheil equation and Ohnaka's model are introduced to the solute profile as shown in Fig. 9. Scheil's equation is derived from the assumption that there is no back-diffusion in solid and a complete homogeneous distribution of elements in the residual liquid. On the contrary, Ohnaka's model considered the back diffusion in solid. The Scheil equation[15] and Ohnaka's model[16] are described as follows,

Scheil's equation: $C_S = kC_0\left(1 - fs\right)^{k-1}$ .... (5)

Ohnaka's equation: $Cs = kC_o\,(1-\Gamma * f_s)^{(k-1)/\Gamma}$ …. (6)

$\Gamma = 1 - Bk/\,(1+B)$ .... (7)

$B = 4\alpha/\,(1+4\,\alpha)$ .... (8)

Where:

C_s : the composition in sloid.

$C_\circ$: the initial alloy composition.

f_s : the solid volume fraction.

K : the partition coefficient to primary γ.

Γ : constant, depending on diffusion.

B : constant, depending on diffusion.

And $\alpha = 4D_S t_S \,/\, \lambda_2^2$ …. (9)

Where:

α: a constant related to the appropriate dendrite arm spacing.

D_s: diffusivity of the solute in solid [m^2/s].

t_s: solidification time [s], (9620s for 1k/min)

λ_2: secondary dendrite arm spacing [μm], (154.91 μm for 3.5 %Re specimen).

And $D_S = D_0 \exp\left(-Q/RT\right)$ …. (10)

Where:

$D_\circ$: Diffusion coefficient (m^2/s), [5.6×10^{-4} for Nb[17] and $8.2*10^{-7}$ for Re[18]].

Q: Activation energy (KJ). [286 for Nb [17] and 255 for Re [18] (1433~1616K)].

R: Gas constant [8.3 J/mole.K].

T: Measuring temperature [K].

According to the above equations, D_s for Nb is 2.955×10^{-13} and 4.383×10^{-15} in case of Re and α is equal to 0.47 for Nb and 0.007 for Re. For both Nb and Re B=0 in Scheil method while in Ohnaka's model B=0.65 for Nb and 0.027 for Re. The distributions of Nb and Re in solid phase with both models are drawn at broken and solid lines, as shown in Fig 11. The composition analysis of Nb is closer to distribution of Ohnaka's model rather than Scheil's model that indicates the back diffusion in □ phase is remarkably takes place at 1K/mm, in case of Nb (Fig. 11). On the other hand, the distribution of Re is closer to the Scheil method than Ohnaka's model, which indicates Re diffuses slower than Nb in primary □̃

The distribution of Nb and Re in liquid phase was evaluated at the cooling rate of 10 K/min. In Fig. 10, the experimental results were plotted and compared with theoretical model in equilibrium conditions as proposed by Clyne-Kurz[19] and Scheil[15]. By using the derivative equation of Clyne-Kurz, the calculated relationship between Nb and Re concentration in residual liquid and fraction of solid was plotted. The equation of Clyne-Kurz is described as follows.[19]

$$C_L = C_0\left\{1-(1-B)f_S\right\}^{(k-1)/(1-Bk)} \qquad \text{.... (11)}$$

Where:

C_L: the chemical analysis of element in residual liquid.

$$\text{And} \quad B = 2\alpha\left\{1-\exp(-1/\alpha)\right\}\exp(-1/2\alpha) \quad \text{.... (12)}$$

According to the previous data, the value of α is 0.23 for Nb and is 0.0034 for Re, where solidification time is 1000s and λ_2 is 72.23 um in case of 10k/min. In case of equilibrium, B is equal to one and B=0 in Scheil method for both Nb and Re. By substituting the value of α and B in the Clyne-Kurz equation, the variation of Nb content in liquid during the solidification of primary γ was calculated. Due to the difficulty to find out the diffusion data of Re in Ni base alloys, it was assumed that the Re element has the same diffusion properties as Nb as the first approximation. By the same way for Nb calculations, the variation of Re content in liquid phase was calculated with the continuity of primary γ solidification. Both of partition coefficient of Nb (K_γ^{Nb}) and Re (K_γ^{Re}) were assumed to be constant during the solidification of primary γ. As shown in Fig. 10, the Nb content in residual liquid increased while in case of Re decreased from 5.8% and 3.4% as the solidification proceed to 14.5% and 1.8% at the fraction of solid increases to 0.75. The eutectic (γ+NbC) starts freezing when Fs reached 0.76, at which the Nb concentration in liquid elevated to about 15%. There were some deviations between the calculated results and each other, and that deviation is originating from the different assuming theories about the diffusion in solid. As shown in Fig. 10. The experimental analysis of Nb is located in between Scheil and Clyne-Kurz lines while Re experimental analysis is rather close for both Shceil and Clyn-Kurz.

Where Scheil and Clyne-Kurz calculated results are close to each other, which indicates Re has a smaller diffusivity in primary γ than that for Nb. According to Wanhong Yang, et al., the dendrite core composition indicates some back diffusion of Ti during the prolonged holding at high temperature. But the diffusion did not produce statistically significant composition change, especially for other solute elements. It seems that the cooling rate of 5 K/min was fast enough to suppress strong back diffusion in the solid [17]. Therefore, at the cooling rate of 10 K/min, the solidification time is shorter than the diffusion time which in turn hinders the back diffusion in solid primary γ phase for Re than Nb. In addition as shown in Fig. 6, the nucleation and growth temperature reduce by increasing the cooling rate. This indicates that the compositions of solid and liquid phase at solid / liquid interface change according the equilibrium phase diagram. The higher (K<1) and lower (K>1) promote the larger microsegregation and higher volume fraction of eutectic phases, as shown in Figs. 6 and 8.

II. 5. References

1. D. M. Stefanesco, ASM HANDBOOK, Vol 15, Casting, May 1992, 815-823.
2. R. E. Schafrik, D. D. Ward and J. R. Gron, Superalloys 718, 625, 706 and Various Dervatives; edited by E.Loria, TMS, 2001.
3. D. F. Paulonis and J. J. SChirra, Superalloys 718,625, 706 and Various Dervatives; edited by E.Loria, TMS, 2001.
4. C. Salama, M. Abdellaoui, Journal of Alloys and Compounds, 306, 2000, 277-284.
5. J. Ruesing, N. Wanderka, U. Czubayko, V. Naundorf, D. Mukherji, J. Roesler, Scripta Materialia, Vol. 46 Issue 3, 1 February 2002, 235 – 240.
6. Q. Feng, T. K. Nandy, S. Tin, T. M. Pollock, Acta Materialia 51, 2003, 269.
7. G. E. Fuchs, B.A. Boutwell, Material Science and Engineering A 333, 2002, 72.
8. G. Appa Rao, Mahendra Kumar, M. Srinivas, D.S. Sarma, Materials Sciense and Engineering A355, 2003, 114-125.
9. S. H. Kang, Y. Deguchi, K. Yamamoto, K. Ogi and M. Shirai and D.M. Stefanescu, Journal of Materials Transactions, vol 45, No. 8, 2004, 2728-2733.
10. Zh. Jingchen and Y. Ping: Superalloys 718, 625, 706 and Various Derivatives, TMS (The Minerals, Metals & Materials Society), 2001, 133-140.
11. P.J. Warren, A. Cerezo, G.D.W. Smith, Material Science and Engineering, A 250, 1998, 88-92.
12. Pierre Caron and Tasadduq Khan, Aerosp. Sci. Technol., vol 3, 1999, 513-523.
13. A.D. Patel and Y. V. Murty: Superalloys 718, 625, 706 and Various Derivatives, TMS (The Minerals, Metals & Materials Society), 2001, 123-131.
14. Wanghong Yang, Wei chen, Keh-Minn Chang, Sarwan Mannan, John deBarbadillo: Superalloys 2000, TMS (The Minerals, Metals & Materials Society), 2000, 75-84.
15. E. Scheil, Bemerkungen zur Schichtkristallbildung: Z. Metallkde, 34, 1942, 70-72.

16. Itsuo Ohnaka, Transactions ISIJ, Vol. 26, 1986, 1045 – 1051.
17. L. Nastac and D. M. Stefanescu: AFS Transactions, 1996, 425-434.
18. M.S.A. Karunaratne, P. Carter, R.C. Reed, Materials Science and Engineering A 281, 2000, 229-233.
19. T. W. Clyne and W. Kurz: Matall. Trans. A Vol. 12 A, 1981, 965- 971.

Table 2 Chemical composition of specimens. (mass %)

% / Alloy	C	Nb	Ti	Cr	Fe	Ni	Mo	Al	Re
St In718	0.06	4.88	0.95	19.45	18.39	52.65	3.06	0.56	--
2.4 Re-In718	0.059	4.76	0.93	18.98	17.83	51.39	2.99	0.55	2.40
3.5 Re-In718	0.058	4.71	0.92	18.77	17.63	50.81	2.95	0.54	3.50
6.0 Re-In718	0.056	4.59	0.89	18.28	17.17	49.49	2.88	0.53	6.00

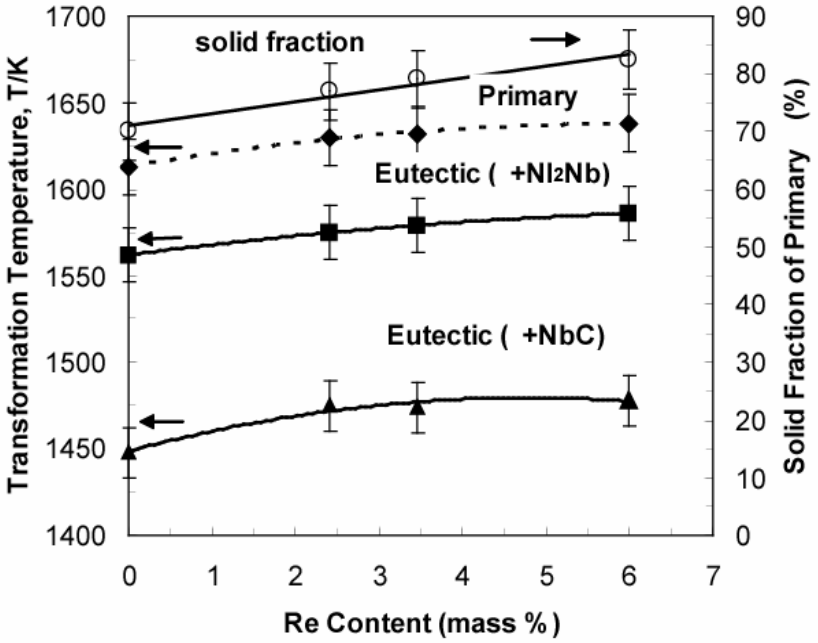

Fig. 2 Influence of Re addition on the transformation temperatures and solid fraction of primary γ.

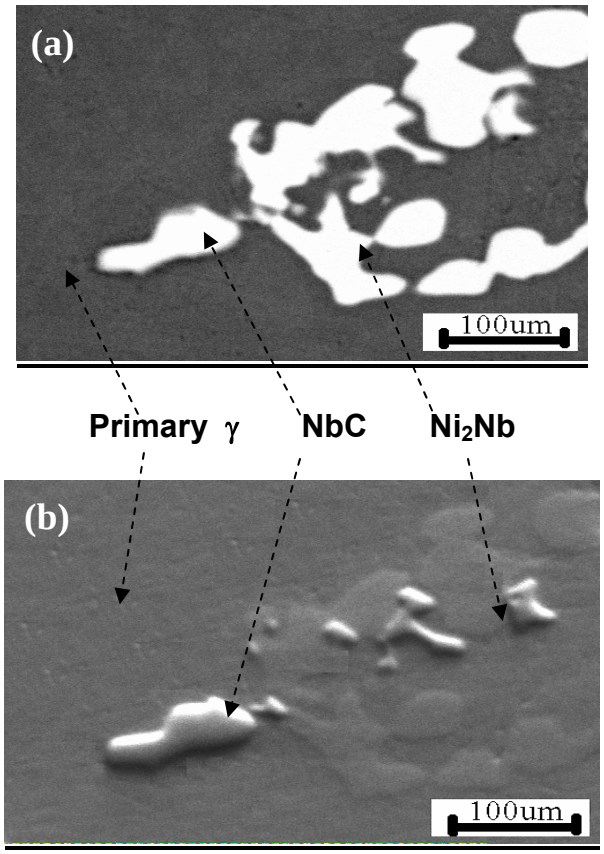

Fig. 3 Back scattered electron (a) and reflected electron (b) photographs for 3.5%Re-Inconel 718 alloy with cooling of 10 K/min

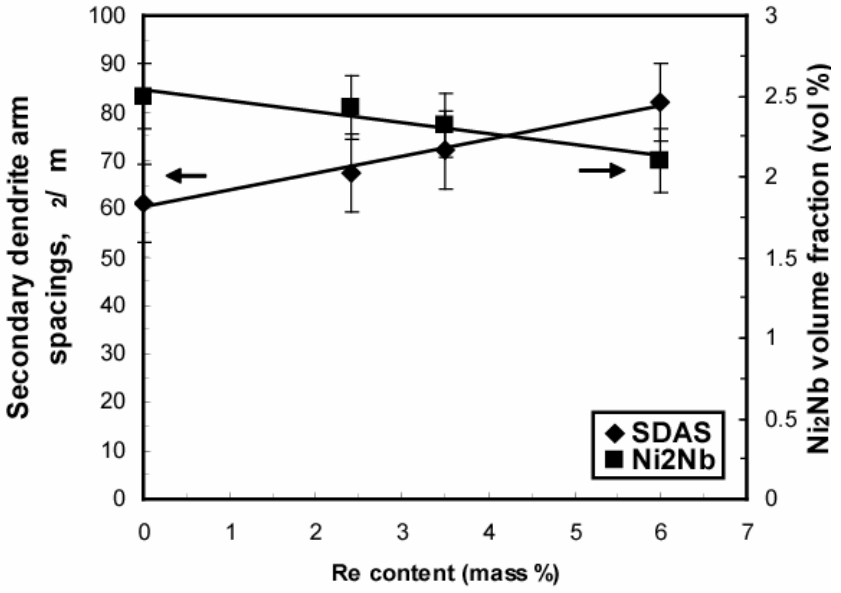

Fig. 4 Dependence of SDAS of primary γ and volume

fraction of Ni_2Nb phase on Re content.

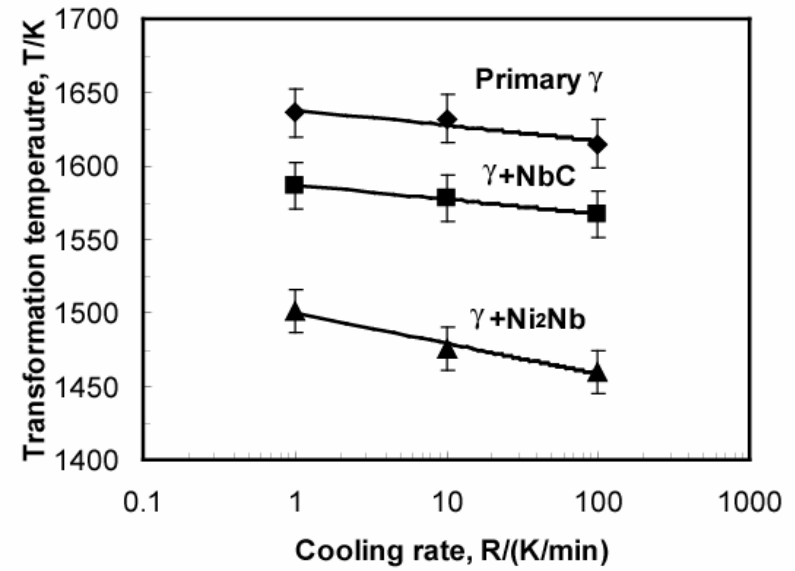

Fig. 5 Influence of cooling rate on the transformation temperatures for 3.5%Re-containing IN718 alloy.

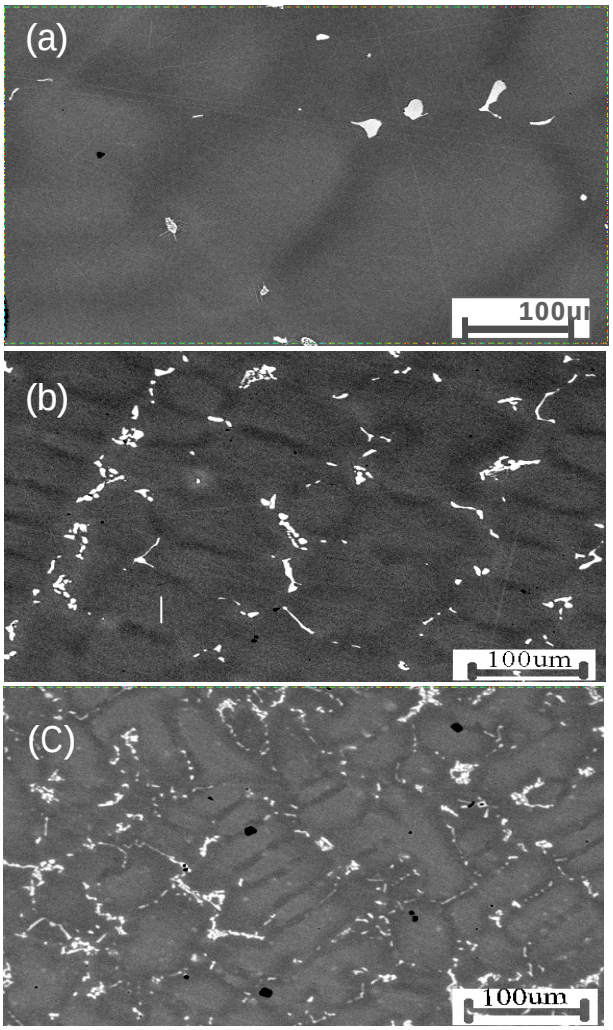

Fig. ٦ The microstructures for 3.5 % Re-containing IN718 alloy solidified at 1 (a), 10 (b) and 100 (c) K/min

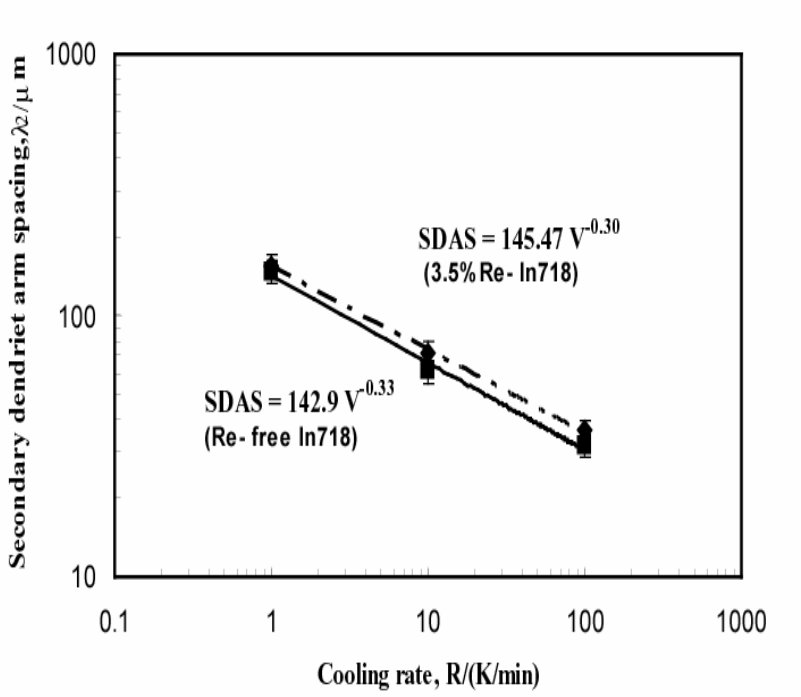

Fig. ٧ Secondary dendrite arm spacing for standard and 3.5%Re-containing IN718 alloys versus variant cooling rates.

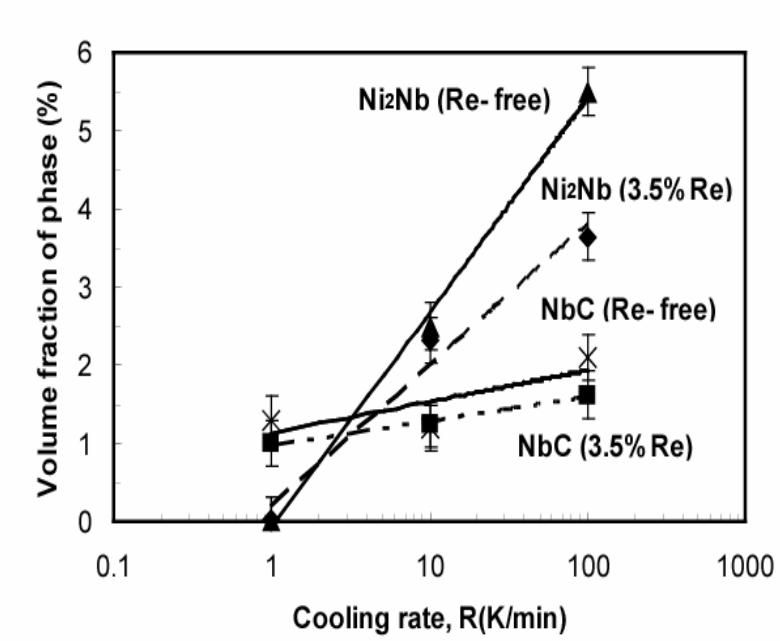

Fig. 8 The relationship between volume fractions of NbC and Ni_2Nb phases and cooling rate.

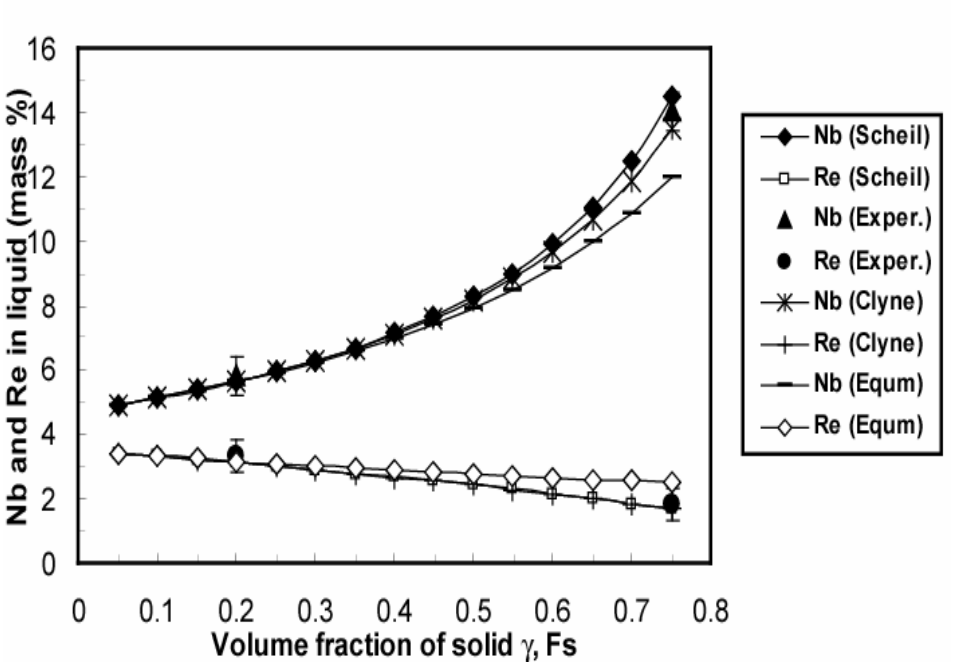

Fig. 9 Distribution of Re and Nb in liquid phase with 10K/min.

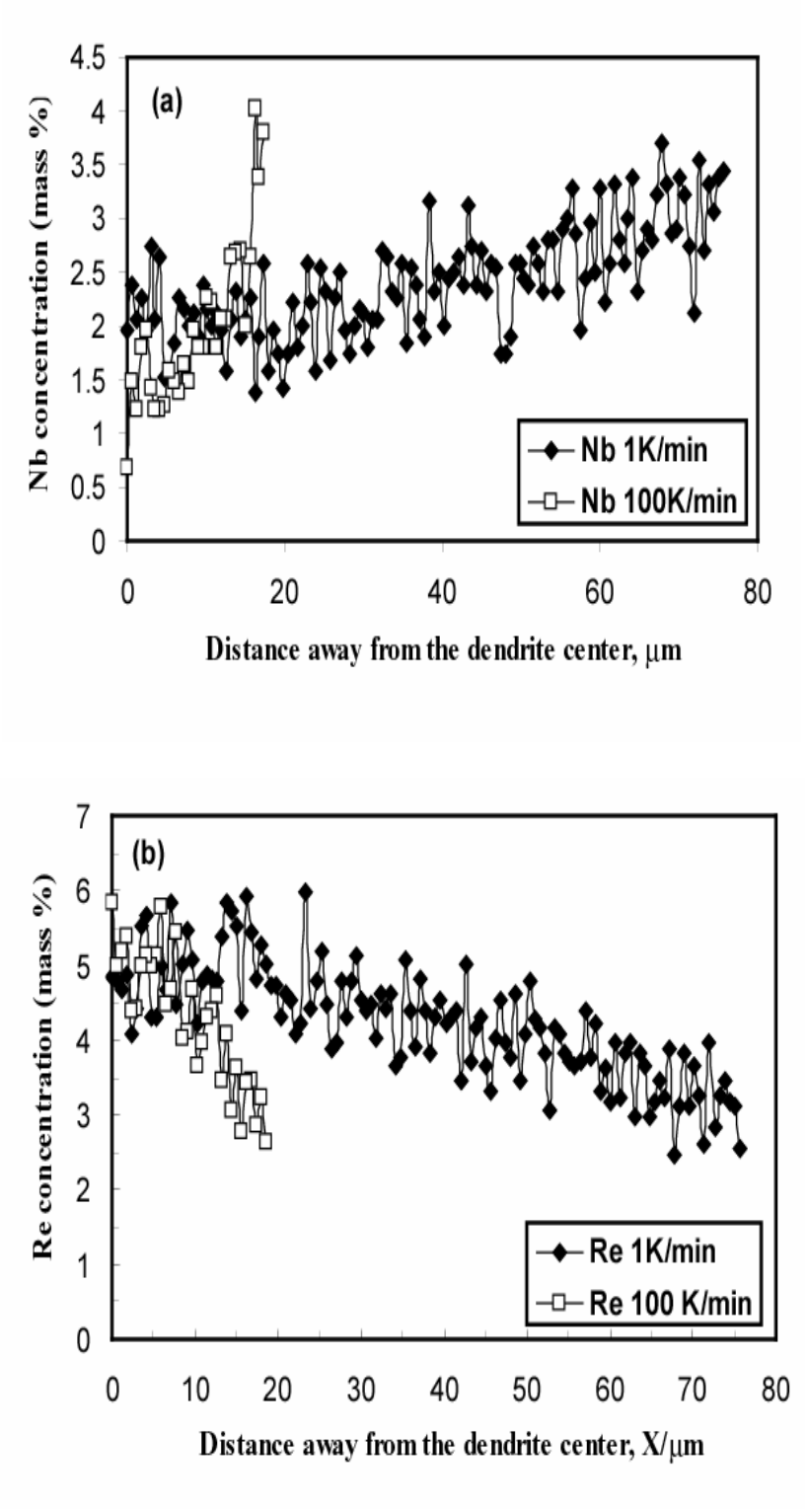

Fig. 10 Distribution of Nb and Re in solid primary γ with 1 and 100 K/min.

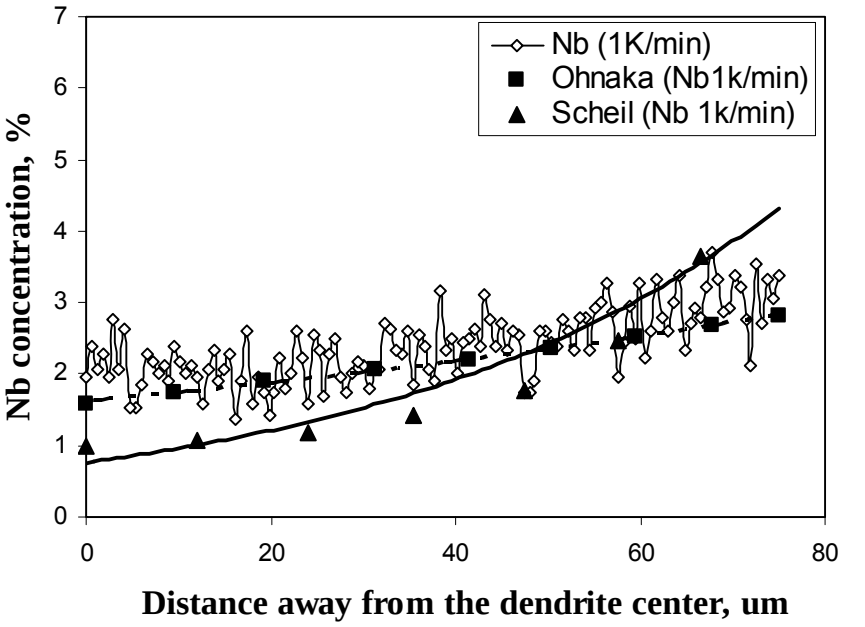

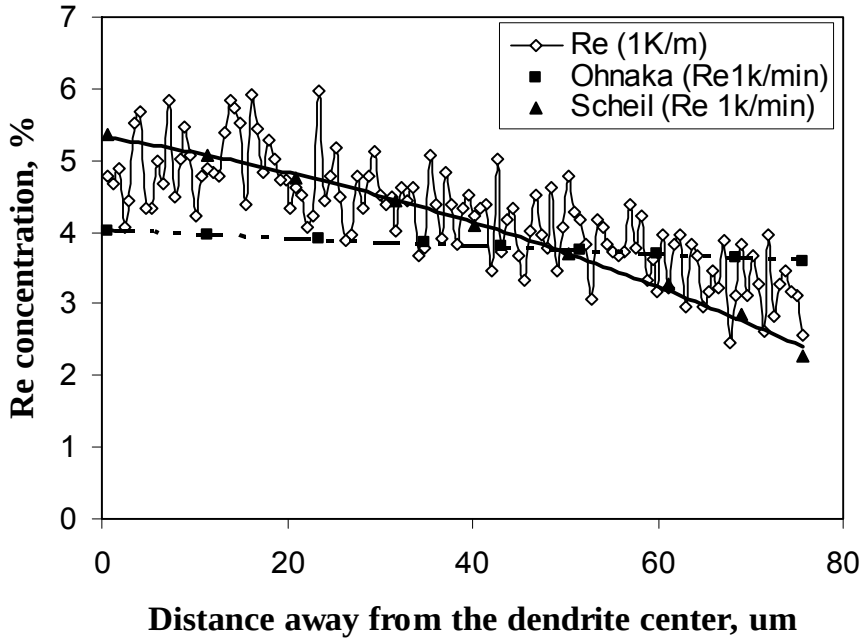

Fig 11 Distribution of Nb and Re in solid primary γ with 1 K/min and compare with Scheil's and Ohnaka's models.